Available online at www.sciencedirect.com

ScienceDirect

Science and Technology of MATERIALS

http://ees.elsevier.com/stmat

Science and Technology of Materials 30 (2018) 86–91

Effect of cooling medium on microstructure evolution and tensile properties of creep-strength-enhanced ferritic steel

C. Pandey [a], N. Saini [a,*], J.G. Thakre [a], M.M. Mahapatra [b], P. Kumar [a]

[a] *Department of Mechanical and Industrial Engineering, Indian Institute of Technology Roorkee, Uttarakhand 247667, India*
[b] *School of Mechanical Sciences, Indian Institute of Technology, Bhubaneswar, Odisha 751013, India*

Received 26 November 2017; accepted 19 January 2018

Abstract

In creep-strength-enhanced ferritic steels, hydrogen-induced cold cracking of weldments is a serious issue. In the present research work, the effect of cooling medium on tensile properties and microstructure evolution of P91 steel weldments has been studied. For water-cooling condition, the diffusible hydrogen metal in deposited metal was measured by the mercury method. The microstructure of weldments in different cooling condition was characterized by using the field-emission scanning electron microscope (FE-SEM) and optical microscope. The fractured tensile test samples were characterized using the FE-SEM. The maximum tensile strength was measured to be 624 MPa for air-cooling medium (very low level of diffusible hydrogen).

Keywords: P91; Diffusible hydrogen; Microstructure; Tensile tests

1. Introduction

In the 21st century, development of clean energy is a key issue that is governed with increase in efficiency of thermal and nuclear power plants. Creep-strength-enhanced ferritic/martensitic steels exhibit better mechanical properties, swelling resistance, and excellent thermal properties compared to the austenitic steels [1–8]. P91 steel is one of the creep-strength ferritic/martensitic steels used in 'Very High-Temperature Reactor' (VHTR) for fabrication of reactor pressure vessels and piping. P91 steel was developed in Oak Ridge National Laboratory (ORNL) with addition of V, Nb, and N in plain 9Cr-1Mo steel. V and Nb were added to form more thermally stabilized fine MX (M: V, Nb; X: C, N) type precipitates that enhanced the creep strength of P91 steel by pinning the dislocation movements [9]. P91 steels are subjected to normalizing and tempering treatment for optimum microstructure evolution that led to enhanced mechanical properties [10–12]. The tempered martensitic microstructure is characterized with Mo, Fe, and Cr-rich coarse $M_{23}C_6$ precipitates along the prior austenite grain boundaries (PAGBs), lath boundaries, and lath packets and fine MX precipitates within laths [1,2]. The schematic diagram of P91 steel in normalized and tempering condition is depicted in Fig. 1(a) and (b), respectively [13,14].

As structural materials for power plant components, the joining of P91 steels was carried out by arc welding processes such as metal arc welding (MAW), gas tungsten arc welding (GTAW), gas metal arc welding (GMAW) and flux core arc welding (FCAW) [4,15,16]. After the welding process, a heterogeneous microstructure was developed across the weldments. The weldments can be classified as weld fusion zone, coarse-grained region, fine-grained region, inter-critical region and over-tempered region depending on the temperature experienced during the welding process [17,18]. The microstructure developed in various zones of weldments depends on cooling rate, cooling medium after the weld thermal cycle which further enhanced by using the post-weld heat treatment (PWHT), and normalizing and tempering (N&T) treatment [19,20].

* Corresponding author.
E-mail addresses: manasfme@gmail.com, nit030078@gmail.com (N. Saini).

https://doi.org/10.1016/j.stmat.2018.01.005

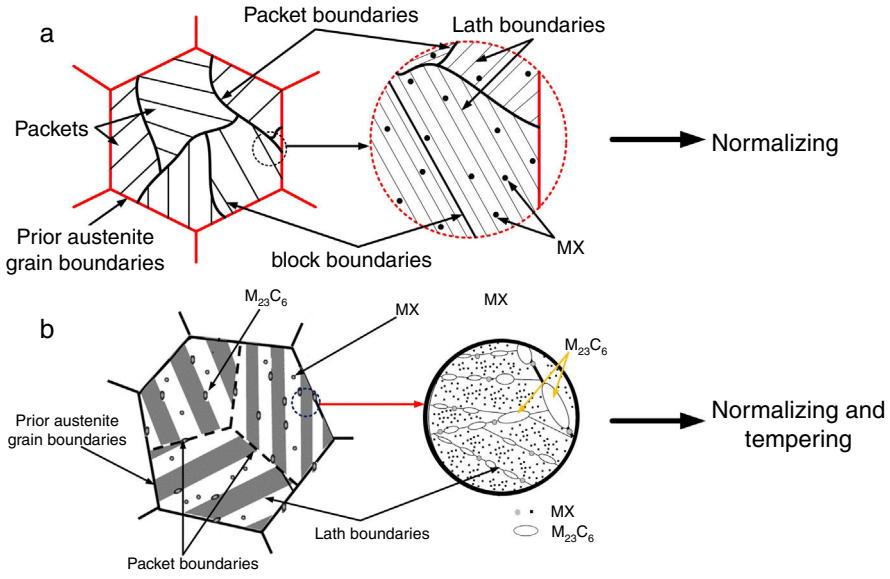

Fig. 1. (a) Schematic evolution of microstructure after: (a) normalizing state, (b) tempering state.

Weldability of P91 steel is a serious issue due to type IV cracking and hydrogen-induced cold cracking [16,21]. During the welding, hydrogen from atmosphere or from the welding consumable trapped into the weld pool. The solubility of hydrogen is more in austenite compared to ferrite while the diffusion coefficient for the austenite is less than the ferrite [22,23]. The dissolution of hydrogen in both ferrite and austenite has been investigated, and the studies reveal that for austenite, hydrogen is favored at octahedral sites and the dissolution energy is smaller than that in ferrite. This is the explanation for larger solubility of hydrogen in austenite than in ferrite (for ferrite, hydrogen is favored at tetrahedral sites) [22]. Hence, the hydrogen particle gets dissolved into austenite phase of HAZ during the weld thermal cycle, and it is not capable to move to diffusion boundary during the cooling cycle because of low-diffusion coefficient. On further cooling, austenite converted into martensite and hydrogen particle remained trapped in the martensite phase. The trapped hydrogen in HAZ and weld zone resulted in hydrogen-induced cracking of P91 weldments.

The hydrogen atom trapped in deposited metal is measured by using the mercury method, vacuum hot extraction, and gas chromatography method, which are the most commonly used methods for diffusible hydrogen measurement [16,24]. The most commonly used is the mercury method because of high reliability and repeatability [16,24–27]. To measure the weldability of steel, Granjon implant test, Tekken test, temper bead welding technique, and controlled thermal severity (CTS) test are most commonly used. The CTS test deals with the control of HAZ hardness by varying the cooling rate. Fydrych et al. [28] have successfully implemented the tempered bead welding (TBW) technique. To determine the HIC in HAZ, Granjon implant test was developed in Institute de Soudure (French Welding Institute) by Henri Granjon.

The present research work deals with the of effect of cooling medium on microstructure evolution and tensile properties of P91 weldments. For water cooling, hydrogen particles in deposited metal were measured by using the mercury method. To study the microstructure evolution, optical microscope and field scanning electron microscope have been utilized.

2. Experimental details

The shielded metal arc welding process was utilized to deposit the weld bead on C&F P91 steel supplied from Bharat Heavy Electricals Limited (BHEL), India. The low-hydrogen welding consumable 9CrMo V-N (AWS ER90S-B9) of diameter 4 mm was used after baking at 300 °C for 2 h to deposit the weld bead. The chemical composition of base metal and welding rod is depicted in Table 1. After bead deposition, one plate is allowed to cool in air, and the other one is cooled in a water environment as per reference [29]. Water quenching was performed to arrest the hydrogen particles in the deposited metal. The diffusible hydrogen present in the deposited metal was measured by the mercury method as per IS:11802-1986 standard. The experimental setup for diffusible hydrogen measurement is shown in Fig. 2 [29].

The schematic of weld assembly used for diffusible hydrogen measurement in mercury method is shown in Fig. 3(a). Test assembly consisted of specimen piece of dimension 30 × 15 × 10 mm and run-on and run-off piece of dimension 45 × 15 × 10 mm. The test assembly was heated at 650 °C for 1 h to remove any bulk hydrogen. After cooling, clean with emery paper. During the welding, the test specimen was placed between run-on piece and run-off piece, and welding is carried out by positioning the test assembly on a copper jig fixture, as shown in Fig. 3(b). The welding parameters used for the bead deposition are depicted in Table 2. Immediately after the welding, the test assembly was quenched in iced water. The run-on piece and run-off piece are broken with the help of vice and hammer, as shown in Fig. 3(c). The center piece was placed at −50 °C in cooling chamber for 3–5 min after 10 s of welding. Subsequently, the test pieces were removed from the cooling chamber

Table 1
Chemical composition of as-received C&F P91 steel, SMAW filler rod, %wt.

Element	Chemical composition, wt%												
	C	Mn	W	S	Si	Cr	Mo	V	N	Ni	Cu	Nb	Ti
C&F P91 steel	0.023	0.689	.0258	0.019	0.193	8.16	0.710	<0.005	<0.02	0.305	0.034	<0.008	<0.02
SMAW filler rod	0.08–0.13	0.40–1.0	–	Max 0.02	0.20–0.50	8–10	0.85–1.1	0.15–0.30	0.03–0.07	0.4–1.0	–	0.04–0.08	–

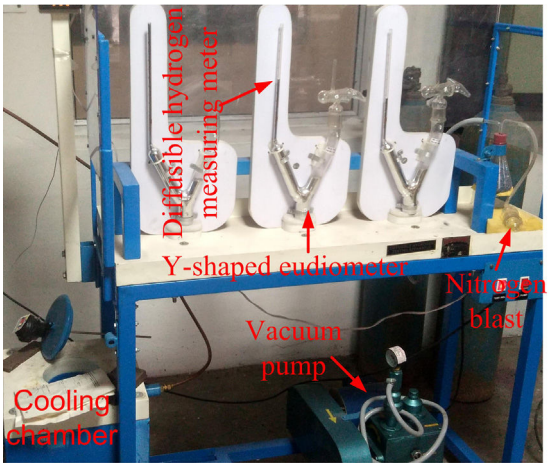

Fig. 2. Experimental set up for diffusible hydrogen measurement.

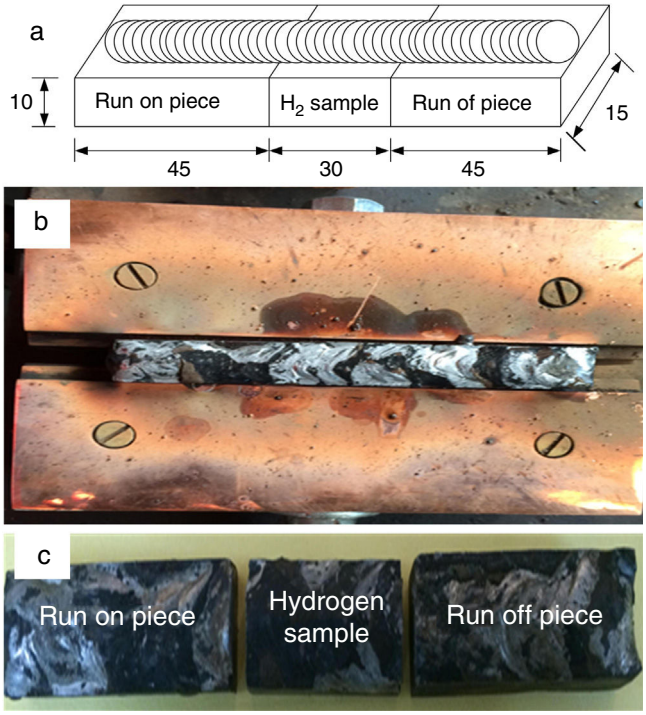

Fig. 3. (a) Schematic of test assembly, (b) specimen hold in copper jig fixture, (c) broken test assembly.

Table 2
Welding process parameter for diffusible hydrogen measurement.

Bead pass	Current (amp)	Voltage (V)	Travel speed (mm/s)	Heat input (kJ/mm)
1	135	27–29	3.20	0.85–0.92

and washed with alcohol and pure ether, and then placed in the glass capsule for drying in the blast of dry nitrogen. After that, the test specimen was admitted through open limb into the Y-tube of mercury apparatus, and limb was closed. Three tests are carried out simultaneously as shown in Fig. 2. The specimen inside the Y-tube is allowed to evolve the hydrogen for 72 h, and it was collected over the mercury at room temperature. The released hydrogen was measured by the volumetric method by using diffusible hydrogen measuring meter as shown in Fig. 2.

The released hydrogen in mercury method was measured with the help of temperature, pressure, and mass of deposited metal. The diffusible hydrogen volume per 100 g of deposited metal is presented in Eq. (1);

$$H_{\text{mercury}} = V_g \frac{273}{273+T} \frac{B-H}{760} \frac{100}{M_2-M_1} \quad (1)$$

where H_{mercury} is diffusible hydrogen per 100 g of deposited metal; V_g is the volume of gas in ml after 72 h; T is the room temperature in C; B is the barometric pressure in mm Hg; H is difference in the heights of mercury levels in two limbs of eudiometer (Y-tube) in mm; M_1 and M_2 are the mass of sample in g before deposition and after removal from mercury apparatus, respectively.

The weld heat input is given by Eq. (2) [30],

$$Q = \frac{\eta X V X I}{TS} \quad (2)$$

where η = arc efficiency (0.75), V = arc voltage, I = welding current, and TS = travel speed.

As per ASTM A 337 standard size, tensile specimen of gauge length and width of 100 mm and 15 mm, respectively, was prepared. The single 100-mm long pass of SMAW bead was deposited over the gauge length by fixing it in copper jig. The average bead height was 1.65 ± 0.13 mm. The welding process parameters remained the same as used for diffusible hydrogen measurement. After the bead deposition, two tensile specimens were quenched in the ice water immediately and then placed in acetone at $-50\,^{\circ}$C for 10 min. The cryogenic condition was implemented to stop the mobility of hydrogen in the weld metal. The other two tensile specimens were allowed to cool in air. After cooling, the samples were subjected to tensile testing on the Universal Testing Machine (UTM) at room temperature and a crosshead speed of 1 mm/min. The schematic of the tensile test specimen is shown in Fig. 4.

A small section was cut from the deposited section for macrostructure and microstructure characterization. For microstructure characterization, the cut section was polished using silicon carbide (SiC) emery paper up to a grit size of 2000.

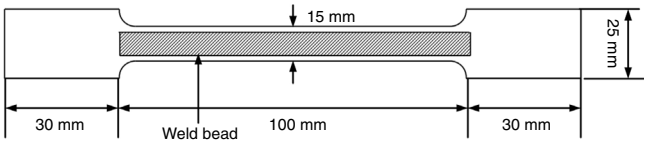

Fig. 4. Schematic of tensile test specimen [16].

After that, cloth polishing with alumina powder was performed to remove paper scratches. The cloth-polished sample was etched in Vilella's reagent (100 ml of ethanol, 1 g of picric acid, and 5 ml of hydrochloric acid). After etching, characterization was carried out using an optical microscope and FE-SEM QUANTA 200.

3. Results and discussion

3.1. As-received material and mechanical properties

Typical secondary electron micrograph of as-received P91 steel is shown in Fig. 5. At low magnification, the microstructure is characterized with the presence of lath boundaries and decoration of precipitates along the boundaries and inside the matrix region. The lath boundaries are mainly decorated with coarse carbide $M_{23}C_6$ type precipitates that are enriched in Cr, Fe, and Mo, while inside the matrix region V, and Nb-rich fine MX precipitates are observed [31,32]. The other precipitates noticed in P91 steel microstructure are Fe, Cr and Mn-rich M_7C_3, Fe-rich M_3C, Cr_2N, and Fe_2C [33]. The secondary electron micrograph at higher magnification shows the distribution of coarse and fine precipitates along the boundaries and inside the matrix region. The average precipitate diameter is measured to be 151 nm by using Image J software.

3.2. Weldments macrostructure

The macrostructure of weldments in water-cooled and air-cooled condition is shown in Fig. 6(a and b). The weld zone and HAZ are clearly seen from the macrograph. In water-cooled condition, the macrostructure consisted of a crack at the center of weld fusion zone. The crack is nucleated as a result of the sudden quenching. The crack is initiated in the weld fusion zone and moves toward the coarse-grained heat-affected zone. It occurred due to high cooling rate. In air-cooled condition, no cracks have been observed in the weld fusion zone or HAZ.

3.3. Weldments microstructure

P91 weldments consisted of weld fusion zone and narrow heat affected zone (HAZ) as shown in Fig. 7. The narrow HAZ consists of subzone: coarse-grained heat-affected zone (CGHAZ), fine-grained heat-affected zone (FGHAZ), and intercritical heat-affected zone (ICHAZ). The optical micrographs of weld fusion zone, CGHAZ, and FGHAZ for both water-cooled and air-cooled conditions are shown in Fig. 7. In water-cooled condition, weld fusion zone consisted of lath martensitic structure. In weld fusion zone high temperature resulted in complete dissolution of precipitates that led to carbon and nitrogen in matrix and finally higher strength and poor toughness martensitic microstructure is formed. In weld fusion zone, some amount of δ-ferrite patches is also seen. In CGHAZ, complete dissolution of precipitates makes the boundaries free from the force and leads to coarse-grain structure formation. In CGHAZ also, some of the δ-ferrite patches were seen. In FGHAZ, the temperature experienced was not sufficient to dissolve all the precipitates that cause a pinning force provided by the undissolved precipitates and led to formation of fine-grained structure. In air-cooled condition, the microstructure obtained for the subzones was completely different from the water-cooled condition. For weld fusion zone, a complete untempered columnar lath structure was formed, as shown in Fig. 7(d). In CGHAZ, a columnar lath structure was formed, as shown in Fig. 7(e). The microstructure obtained in FGHAZ also consisted of columnar lath structure as obtained for the as-received C&F P91 steel. In air-cooled condition, the δ-ferrite patches were not observed, which make the structure uniform.

The optical micrograph at higher magnification also shows the presence of ferrite patches in the weld fusion zone of water-cooled sample. The patches are observed in different size and shape, as shown in Fig. 8(a). The SEM micrograph also confirms the presence of ferrite patches, as shown in Fig. 8(b). The ferrite patches make the microstructure soft (poor hardness) and also reduce the mechanical properties of the weldments [34].

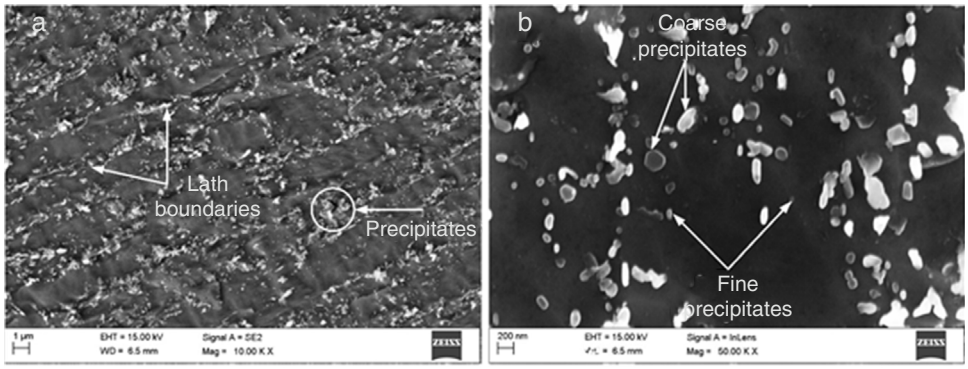

Fig. 5. Secondary electron micrograph of as-received P91 steel (a) at lower magnification of 5000×, (b) at higher magnification of 50,000×.

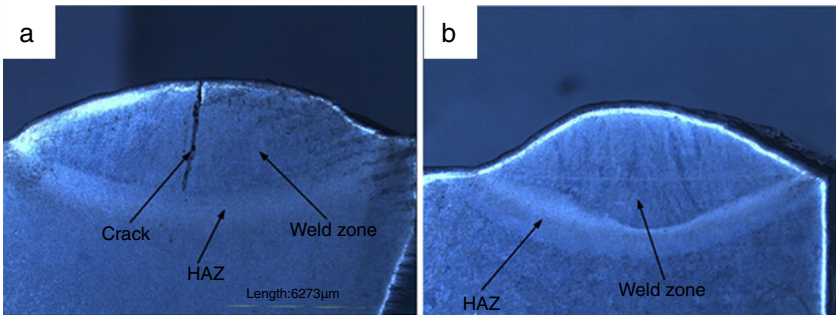

Fig. 6. Macrostructure of P91 weldments (a) water cooled, (b) air cooled.

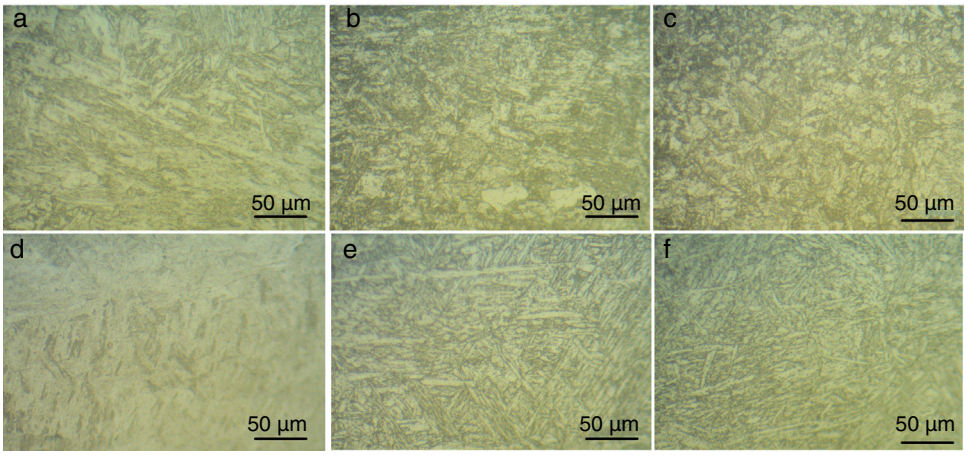

Fig. 7. Optical micrograph of P91 weldments in water cooled (a) weld fusion zone, (b) CGHAZ, (c) FGHAZ; in air cooled condition (d) weld fusion zone, (e) CGHAZ, (f) FGHAZ.

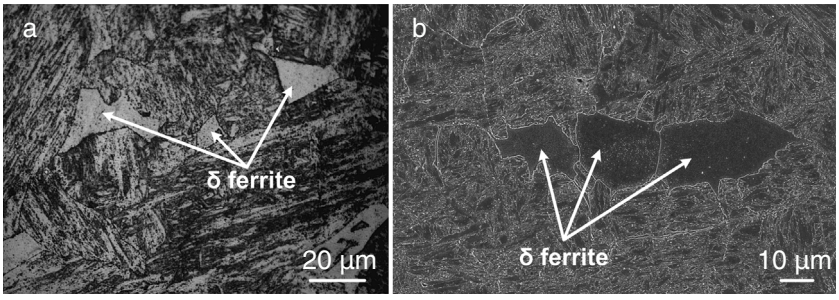

Fig. 8. Micrograph of weld fusion zone in water cooled condition (a) optical, (b) SEM.

3.4. Diffusible hydrogen measurement

Diffusible hydrogen was measured by mercury method as per reference [24]. The diffusible hydrogen was measured for water-cooled condition. In air-cooled condition, the diffusible hydrogen was allowed to diffuse into the atmosphere. For diffusible hydrogen measurement, three trials have been performed, with results of 3.92 ml/100 g, 3.89 ml/100 g, and 3.94 ml/100 g. The average value of diffusible hydrogen was 3.92 ml/100 g.

3.5. Tensile properties

The engineering stress–strain curve for both media is shown in Fig. 9. For water-cooled medium, the cooling was carried out as per reference [16]. For cooling air, simple air cooling was carried out after the welding. In case of air-cooled medium, tensile strength and percentage elongation were found to be more compared to water-cooled condition. The tensile strengths measured for air-cooled and water-cooled media were 606 MPa and 331 MPa, respectively. Percentage elongation was measured to be 6.38% and 8.71% for water-cooled and air-cooled, respectively. The strength mainly depends on the microstructure, diffusible hydrogen content, and residual stress developed after the welding. The microstructure obtained after the cooling was almost similar for both the cases except the presence of δ-ferrite patches in water-cooled condition. The other difference was the presence of diffusible hydrogen in water-cooled condition. The microstructure and the presence of diffusible hydrogen content in weldments led to lower strength of water-cooled condition.

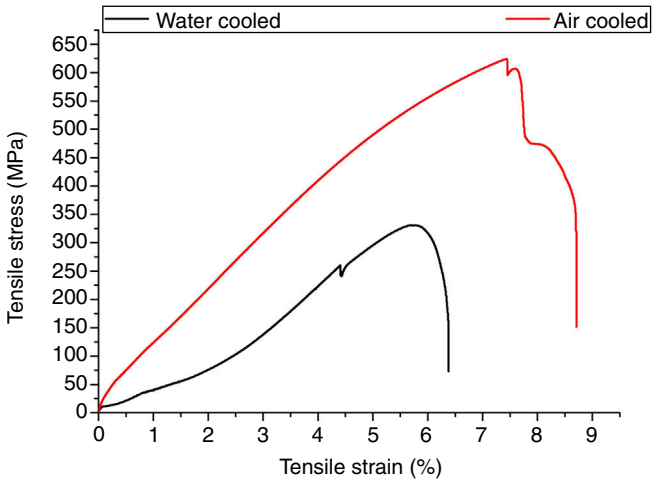

Fig. 9. Engineering stress–strain curve.

In water-cooled condition, sudden quenching in water also led to crack formation in weld fusion zone as shown in the micrograph.

4. Conclusions

From the research, the following conclusions can be drawn:

The as-received C&F P91 steel consisted of tempered martensitic microstructure with coarse $M_{23}C_6$ precipitates along the PAGBs and lath boundaries while fine MX precipitates inside the matrix region.

The microstructure obtained for P91 weldments in water-cooled condition was characterized with presence of untempered columnar laths with δ-ferrite patches, while in the case of air-cooled condition, δ-ferrite patches were found to be absent.

The diffusible hydrogen measured for water-cooled condition was 3.92 ml/100 g of deposited metal.

In water-cooled condition, the arrested hydrogen in the weld fusion zone results in poor strength and ductility as compared to the air-cooled condition in which a negligible amount of diffusible hydrogen is present. In water-cooled condition, sudden quenching also leads to the formation of cracks that might be the cause of poor strength in water-cooled condition.

Conflict of interest

The authors declare that there is no conflict of interest regarding the publication of this paper.

References

[1] J. Hald, Int. J. Press. Vessels Pip. 85 (2008) 30.
[2] K.S. Chandravathi, K. Laha, K.B.S. Rao, S.L. Mannan, Mater. Sci. Technol. 17 (2001) 559.
[3] A. Aghajani, C. Somsen, G. Eggeler, Acta Mater. 57 (2009) 5093.
[4] B. Arivazhagan, S. Sundaresan, M. Kamaraj, J. Mater. Process. Technol. 209 (2009) 5245.
[5] D.R. Barbadikar, G.S. Deshmukh, L. Maddi, K. Laha, P. Parameswaran, A.R. Ballal, D.R. Peshwe, R.K. Paretkar, M. Nandagopal, M.D. Mathew, Int. J. Press. Vessels Pip. 97 (2015) 132–133.
[6] Y. Wang, R. Kannan, L. Zhang, L. Li, Weld. J. 96 (2017) 203.
[7] M. Yoshino, Y. Mishima, Y. Toda, H. Kushima, K. Sawada, K. Kimura, Mater. High Temp. 25 (2005) 5.
[8] M. Zubairuddin, S.K. Albert, M. Vasudevan, S. Mahadevan, V. Chaudhri, V.K. Suri, Mater. Manuf. Processes 31 (2016) 366.
[9] C. Pandey, M.M. Mahapatra, P. Kumar, R.S. Vidyrathy, A. Srivastava, Mater. Sci. Eng. A 695 (2017) 291.
[10] C. Pandey, A. Giri, M.M. Mahapatra, Mater. Sci. Eng. A 657 (2016) 173.
[11] C. Pandey, M. Mahapatra, Proc. Inst. Mech. Eng. Part E: J. Process Mech. Eng. 664 (2016) 58.
[12] C. Hurtado-noreña, C.A. Danón, M.I. Luppo, P. Bruzzoni, Procedia Mater. Sci. 8 (2015) 1089.
[13] N. Saini, C. Pandey, M.M. Mahapatra, R.S. Mulik, Mater. Sci. Eng.: A 711 (2018) 37.
[14] N. Saini, C. Pandey, M.M. Mahapatra, R.S. Mulik, Eng. Fail. Anal. 85 (2018) 104.
[15] T. Watanabe, M. Tabuchi, M. Yamazaki, H. Hongo, T. Tanabe, Int. J. Press. Vessels Pip. 83 (2006) 63.
[16] C. Pandey, M.M. Mahapatra, P. Kumar, N. Saini, J. Eng. Mater. Technol. 139 (2017) 1.
[17] C. Pandey, M.M. Mahapatra, P. Kumar, A. Giri, Met. Mater. Int. 23 (2017) 900.
[18] C. Pandey, A. Giri, M.M. Mahapatra, P. Kumar, Met. Mater. Int. 23 (2017) 148.
[19] C. Pandey, M.M. Mahapatara, P. Kumar, N. Saini, J. Manuf. Processes 31 (2018) 247.
[20] C. Pandey, M.M. Mahapatra, P. Kumar, N. Saini, Mater. Sci. Eng. A 712 (2018) 720.
[21] N. Saini, C. Pandey, M. Mohan, Int. J. Hydrogen Energy 42 (2017) 17328.
[22] E.J. Song, H.K.D.H. Bhadeshia, D.W. Suh, Corros. Sci. 77 (2013) 379.
[23] J. Cermak, L. Kral, J. Alloys Compd. 586 (2014) 129.
[24] C. Pandey, N. Saini, M.M. Mahapatra, P. Kumar, Int. J. Hydrogen Energy (2016).
[25] D. Fydrych, A. Świerczyńska, G. Rogalski, Metall. Ital. 107 (2015) 47.
[26] D. Fydrych, G. Rogalski, Weld. Int. 25 (2011) 166.
[27] D. Fydrych, J. Łabanowski, 2015.
[28] D. Fydrych, J. Łabanowski, G. Rogalski, Pol. Marit. Res. 20 (2013) 67.
[29] C. Pandey, N. Saini, M.M. Mahapatra, P. Kumar, Int. J. Hydrogen Energy 41 (2016) 17695.
[30] C. Pandey, A. Giri, M.M. Mahapatra, Int. J. Steel Struct. 16 (2016) 333.
[31] C.G. Panait, A. Zielinska-Lipiec, T. Koziel, A. Czyrska-filemonowicz, A.F. Gourgues-Lorenzon, W. Bendick, Mater. Sci. Eng. A 527 (2010) 4062.
[32] C. Pandey, M.M. Mahapatra, P. Kumar, N. Saini, Mater. Sci. Eng. A 685 (2017) 39.
[33] C. Pandey, M.M. Mahapatra, P. Kumar, N. Saini, Trans. Indian Inst. Met. (2017).
[34] C. Pandey, M.M. Mahapatra, P. Kumar, N. Saini, J.G. Thakre, R.S. Vidyarthy, H.K. Narang, Arch. Civil Mech. Eng. 18 (2018) 713.